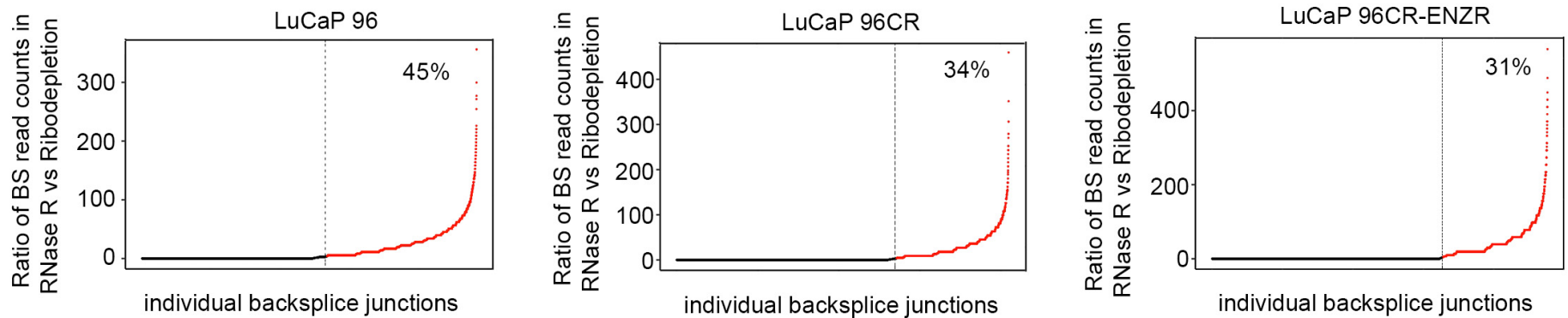
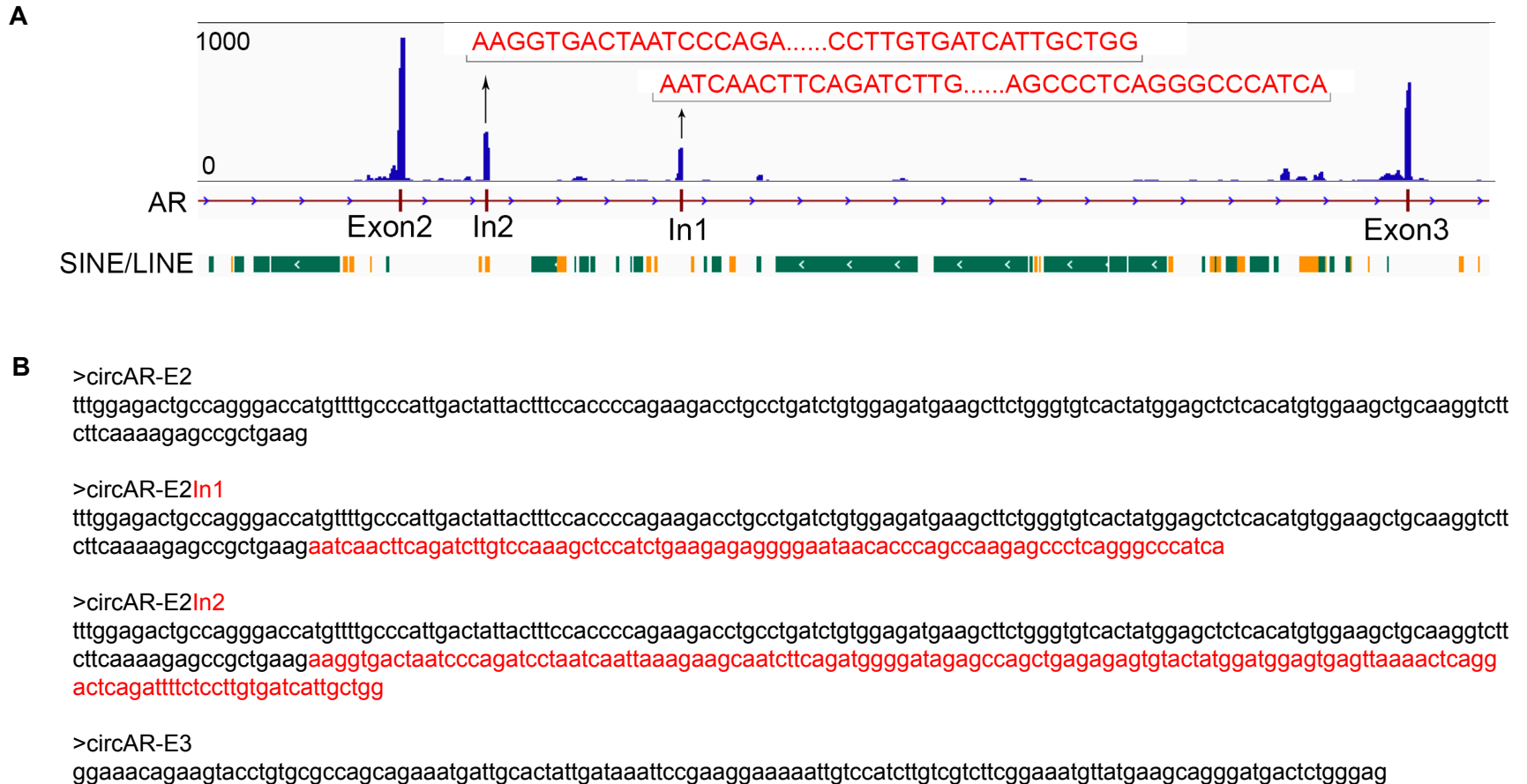


**Figure S1. *In silico* validation of circARs.** RNA-seq reads from SU2C cohort were aligned to conjoined backsplice junctions using STAR and displayed on IGV. Shown in the figure are from one representative sample. Blue bars below the nucleotide sequence represent the exons. Red arrows indicate the location of primers for PCR analysis.



**Figure S2. Enrichment of backsplice junctions after RNase R treatment.** Scatter plots showing that the ratio of backsplicing read counts (normalized to total splicing read counts) in RNase R vs ribodepletion RNA-seq for each junction detected in respective ribodepletion-seq datasets. The vertical dotted lines separate the backsplice junctions without enrichment  $< 5$  folds (left side) from the ones with enrichment  $\geq 5$  folds (right side). The x axis represents individual backsplice junctions ranked according to their read count ratio in RNase R vs ribodepletion RNA-seq.



**Figure S3. Read coverage of RNase R-seq in the circAR genomic region and the full sequences of 4 most abundant circARs.** (A) The read coverage in exon 2 to exon 3 region of the AR genomic locus from RNase R-seq. In1 and In2 are two new cryptic exons in circARs. Eighteen nucleotide sequences at each end of In1 and In2 are shown to indicate the start and end positions of In1 and In2. The SINE/LINE repeats flanking the circularized exons are indicated at the bottom. Green bars indicate the leftward repeats, and orange bars indicate the rightward repeats. (B) The full sequence of the four most abundant circARs.

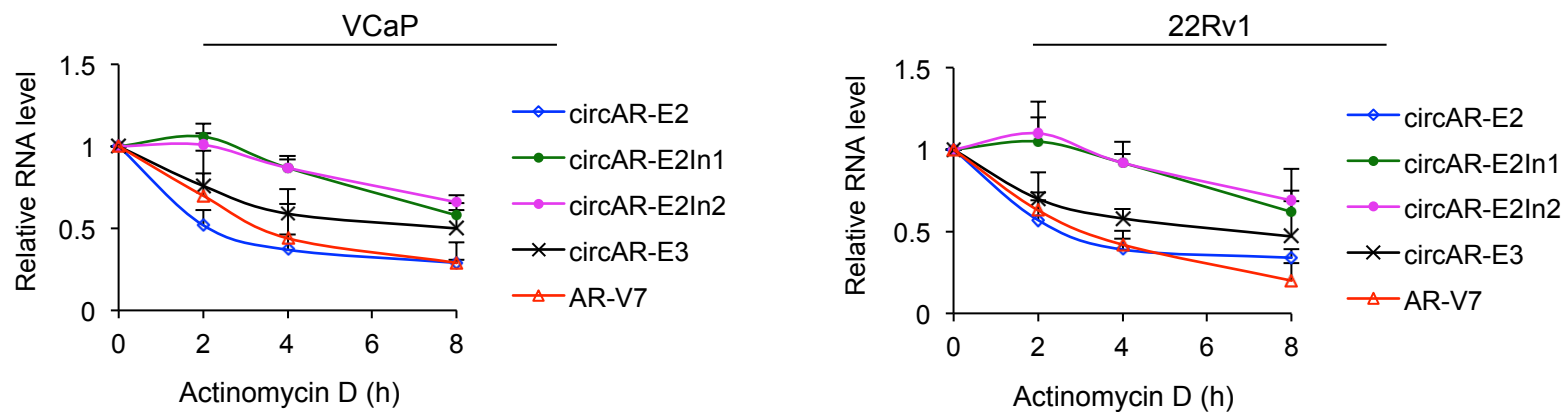


**Figure S4. Stability of circARs relative to AR-V7 mRNA.** RT-qPCR showing a trend of higher stability of circAR-E2In1, circAR-E2In2, and circAR-E3 than the linear AR-V7 transcript but a similar stability of circAR-E2 and AR-V7 in VCaP and 22Rv1 cells. Actinomycin D, 5  $\mu$ M.

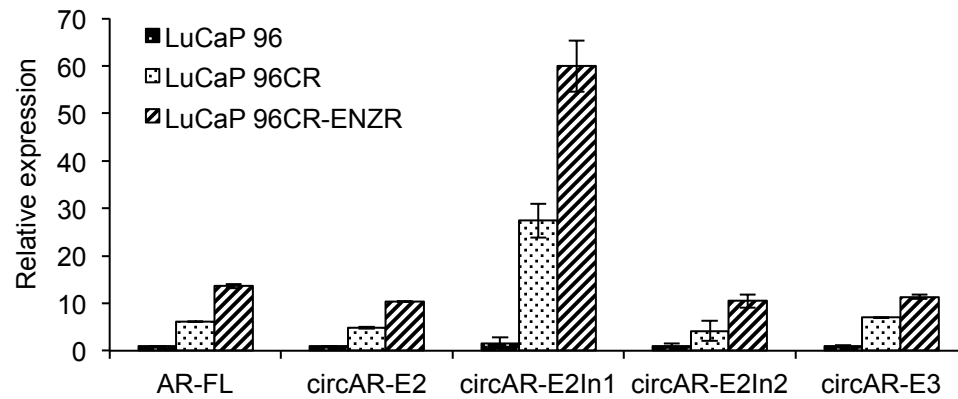


**Figure S5.** Progressive upregulation of AR and circARs during progression of LuCaP 96 PDX from hormone naïve to castration resistance and subsequently to enzalutamide resistance. The normalized levels of each AR transcript detected by RT-qPCR are expressed relative to the mean level of that AR transcript in the hormone-naïve LuCaP 96 tumor.

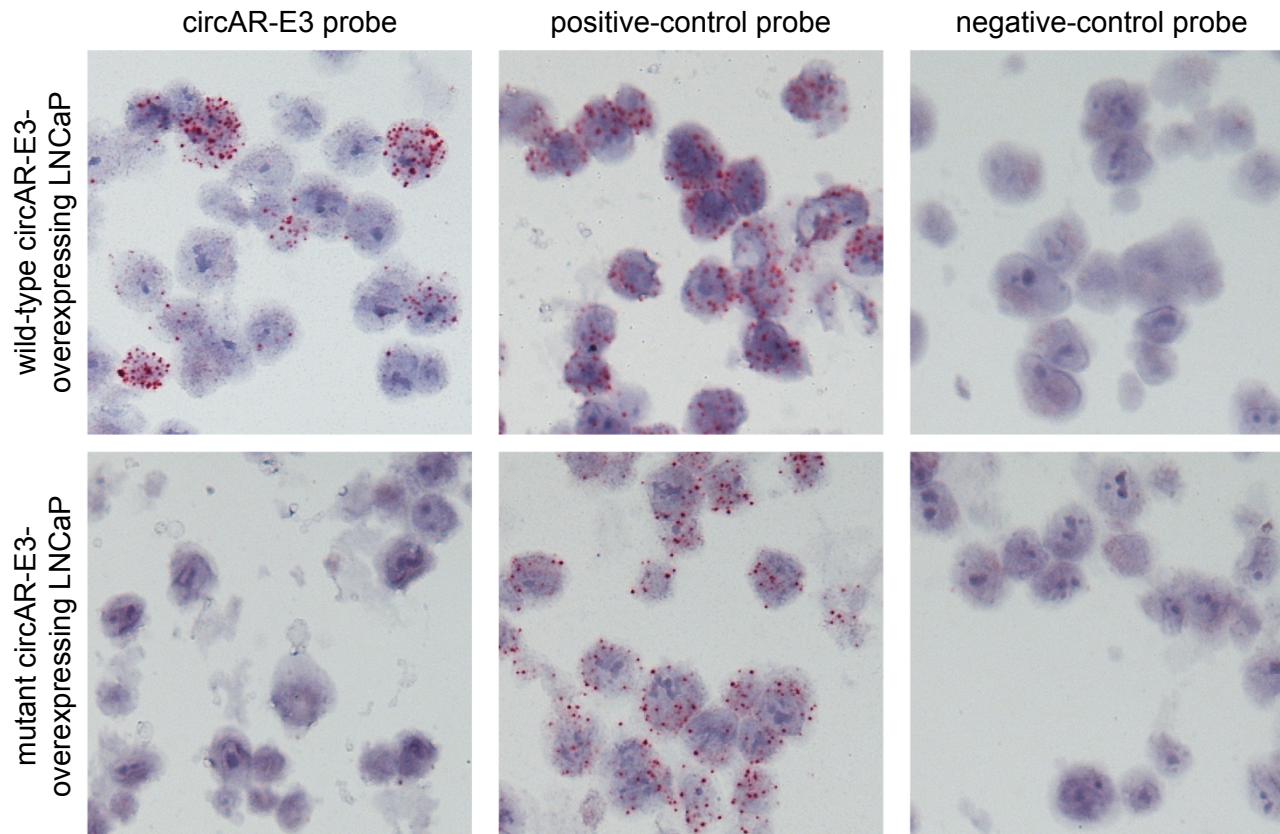


**Figure S6. Validation of the specificity of the circAR-E3 BaseScope probe.** LNCaP cells were transiently transfected with wildtype or mutant (no circularization due to mutated splice donor and acceptor) circAR-E3 expression construct. CircAR-E3 expression was only detectable in wildtype circAR-E3-overexpressing LNCaP cells. The positive and negative control probes were from the BaseScope assay kit.

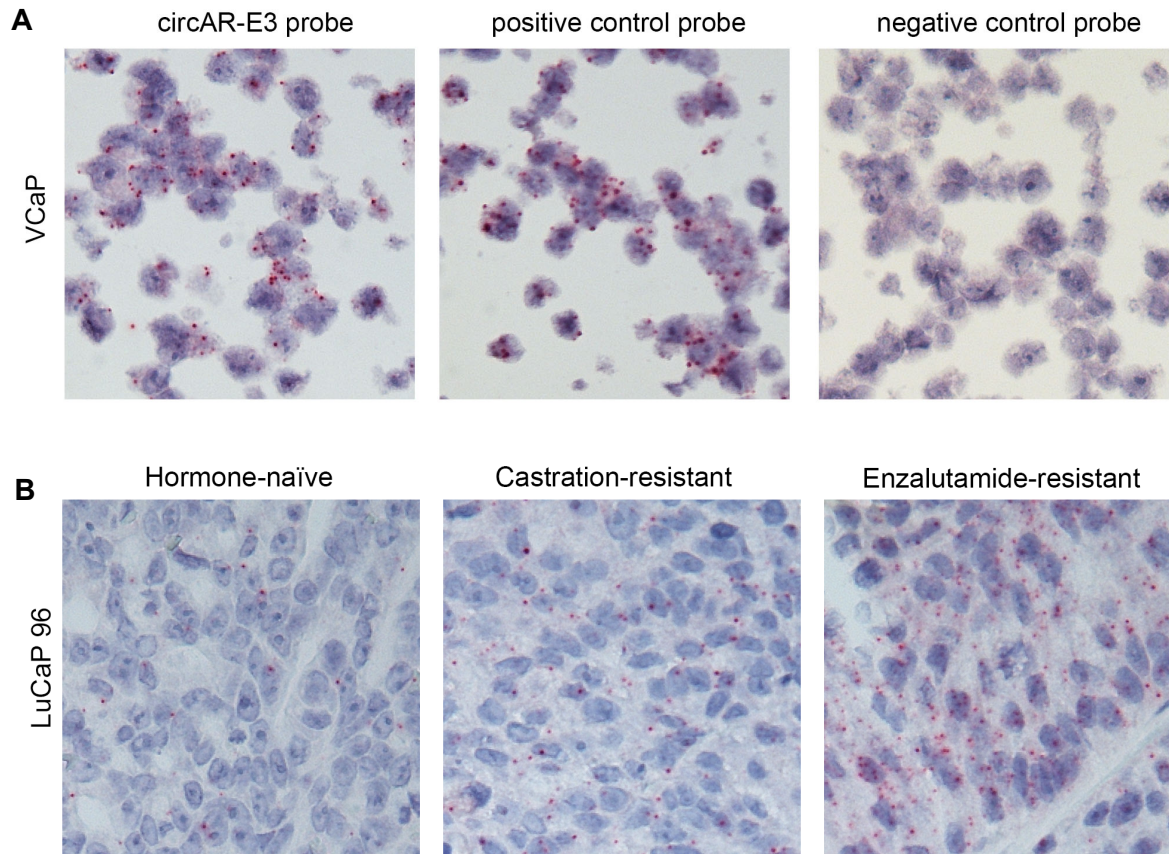


**Figure S7. BaseScope RISH detection of circAR-E3 in VCaP cells and LuCaP 96 PDX tumors. (A)** RISH assay with the circAR-E3 probe as well as the positive and negative control probes in VCaP cells. **(B)** RISH assay with the circAR-E3 probe showing progressive upregulation of circAR-E3 during progression of LuCaP 96 PDXs from hormone naïve to castration resistance and subsequently to enzalutamide resistance.

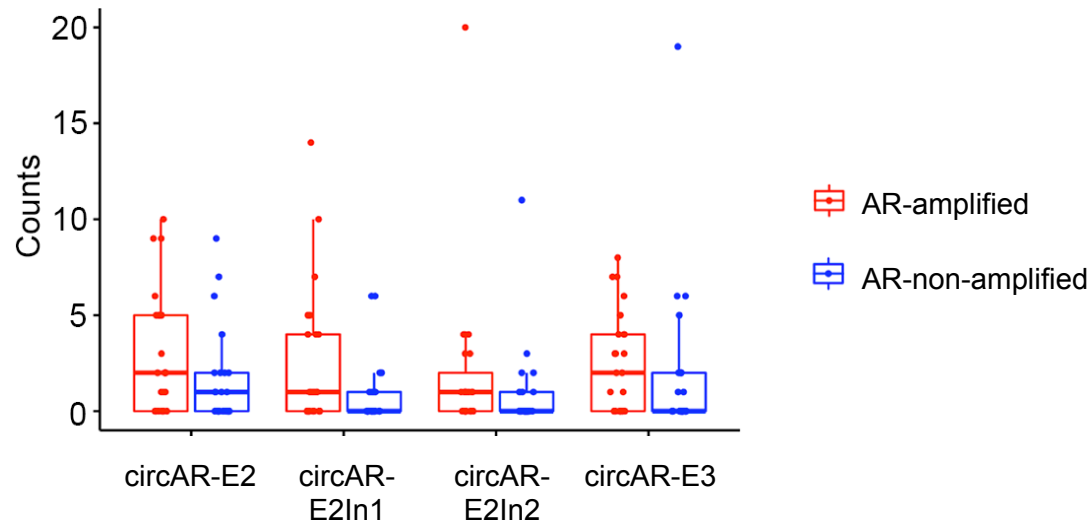


**Figure S8. Detection of circARs in both AR-amplified and –non-amplified mCRPC samples.** The boxplots show the read counts for each circAR in AR-amplified (n = 23) or -non-amplified mCRPC samples (n = 23) in the SU2C cohort with known AR copy number status. The rectangles span from the first to the third quartiles of read counts. The line inside of each rectangle represents the median of the counts, and vertical lines above and below the rectangle show the maximum and minimum counts.



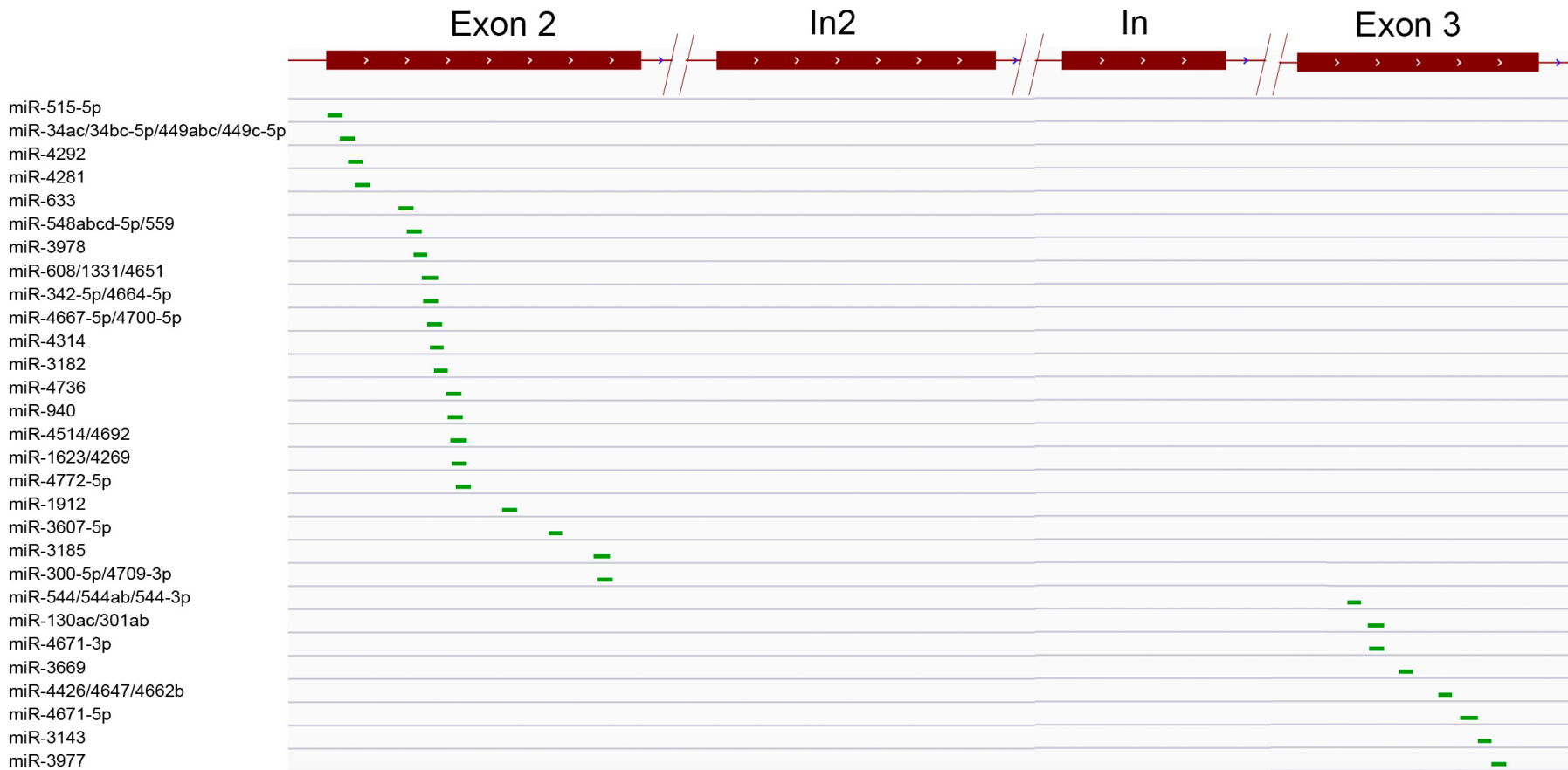


**Figure S9. miRNA binding sites in circAR regions.** AGO-PAR-CLIP-seq data showing miRNA binding sites in AR exon 2 and exon 3 but not in In1 or In2 cryptic exon.